ChemComm

COMMUNICATION

View Article Online
View Journal | View Issue

Cite this: *Chem. Commun.*, 2014, **50**, 9707

Received 20th May 2014,
Accepted 13th June 2014

DOI: 10.1039/c4cc03842h

www.rsc.org/chemcomm

Cu nanoclusters supported on nanocrystalline SiO_2–MnO_2: a bifunctional catalyst for the one-step conversion of glycerol to acrylic acid†

Bipul Sarkar,[a] Chandrashekar Pendem,[a] L. N. Sivakumar Konathala,[a] Ritesh Tiwari,[a] Takehiko Sasaki[b] and Rajaram Bal*[a]

A material consisting of highly dispersed Cu nanoclusters anchored on nanocrystalline SiO_2–MnO_2 has been prepared, and was found to act as a bifunctional catalyst for the one- step conversion of glycerol to acrylic acid using H_2O_2. Under optimized conditions a glycerol conversion of 77.1%, with 74.7% selectivity for acrylic acid, was achieved after 30 h reaction time.

As petroleum reserves diminish, researchers are trying to develop new ways to utilize renewable resources as feedstocks for the generation of energy and production of chemicals, with the aim of lowering CO_2 emissions and fossil-fuel dependency.[1] Much attention has been focused on developing green catalytic processes, in order to convert bio-renewable feedstocks into commodity chemicals and clean fuels. Glycerol is recognized as one of the most promising building blocks for the synthesis of fine chemicals from renewable sources.[2] It is obtained as a by-product of different processes, like soap manufacture, fatty acid production, fatty ester production, microbial fermentation[3] and transesterification, or the production of biodiesel. In order to improve the biofuel economy and put this waste stream to good use, it is necessary to develop new catalytic routes to convert glycerol into value-added chemicals. Therefore, the development of new applications of glycerol will boost the entire glycerol industry. The single-step production of acrylic acid from glycerol is one of the most promising options.

Acrylic acid is a highly important chemical, and almost 4.4 million metric tons per annum are produced as part of the global petrochemical business, with an average revenue of nearly $7 billion per year as of 2011. Acrylic acid is largely employed by the chemical industry for the production of super-absorbers, polymers, adhesives, paints, plastics, rubber, detergents, *etc.* and more than one billion kilograms are produced annually.[4] The entire commercial quantity of acrylic acid is produced *via* a two-stage gas phase oxidation of propylene monomers in air. Here, acrolein is initially formed, followed by the oxidation of the acrolein to acrylic acid. Since the propylene market price is closely tied to crude oil prices due to the use of crude oil derivatives as the feedstock for making propylene, use of alternative feedstocks for making acrylic acid is considered to be a viable option. Various catalysts like γ-Al_2O_3, SiO_2 and TiO_2 have been applied[5] for the direct conversion of glycerol to acrolein, but in most cases the product yield is very low. Metal oxides from the Group II and Group III transition series, *e.g.* Nb_2O_5, WO_3/ZrO_2, metal phosphates, molecular sieves like SAPOs and zeolites have also been used for the conversion of glycerol to acrolein.[6] There are few reports[7] where the two-step production of acrylic acid from glycerol has been presented. Shima *et al.*[7a] described a two-step process, which includes the dehydration of an aqueous solution of glycerol over an alumina base catalyst, to get an acrylic acid yield of ~60%. Although a single oxidation step conversion of glycerol to acrylic acid was reported by Jean-Luc Dubois *et al.*[7c] using molecular oxygen over a plate heat exchanger at 250 °C to 350 °C, the yield was very low. Recently, Trevisanut *et al.* and Ueda *et al.* reported the single step conversion of glycerol to acrylic acid, again with a very poor yield.[8] Herein, we present the single-step conversion of glycerol to acrylic acid over Cu nanoclusters supported on nanocrystalline SiO_2–MnO_2. The hydrothermally prepared Cu/SiO_2–MnO_2 catalyst achieves a glycerol conversion of 77.1% with 74.7% acrylic acid selectivity, and a TOF (turnover frequency) value of 32.9 h^{-1} was achieved. To the best of our knowledge, there is no report on the single-step conversion of glycerol to acrylic acid with such high conversion and selectivity.

The Cu nanoclusters supported on nanocrystalline SiO_2–MnO_2 catalyst was prepared by modifying our own preparation method (in ESI†).[9] The amount of Cu present in the catalyst was estimated by inductively coupled plasma atomic emission spectra (ICP-AES). It was found that 0.9 wt% Cu was present in the catalyst, and so the catalyst was denoted as 0.9%Cu/SiO_2–MnO_2. The powder X-ray

[a] *Catalytic Conversion & Processes Division, CSIR-Indian Institute of Petroleum, Dehradun 248005, India. E-mail: raja@iip.res.in; Fax: +91 135 2660202; Tel: +91 135 2525797*

[b] *Department of Complexity Science and Engineering, The University of Tokyo, Kashiwanoha, Kashiwa-shi, Chiba 277-8561, Japan*

† Electronic supplementary information (ESI) available. See DOI: 10.1039/c4cc03842h

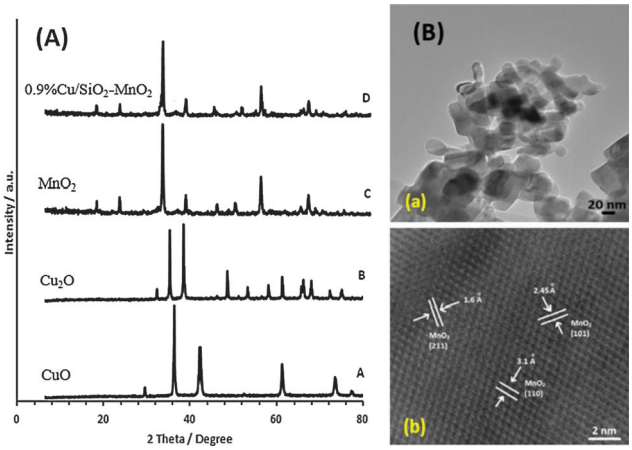

Fig. 1 (A) X-ray diffraction patterns for commercial CuO, Cu_2O, MnO_2 and the prepared 0.9%Cu/SiO_2–MnO_2. (B) TEM images of the prepared 0.9%Cu–SiO_2–MnO_2 at (a) low magnification and (b) high magnification.

diffraction (XRD) pattern of the 0.9%Cu/SiO_2–MnO_2 catalysts is shown in Fig. 1A. The standard diffraction patterns for Cu_2O and CuO are also shown for reference. All peaks for 0.9%Cu/SiO_2–MnO_2 (Fig. 1A) are attributed to those of the crystalline α-MnO_2,[10] which is in accordance with the JCPDS card, No. 44-0141. No XRD peaks attributed to either metallic Cu or its oxides were observed for the sample of 0.9%Cu/SiO_2–MnO_2, which indicates the presence of very small Cu species over the SiO_2–MnO_2 oxide surface. The morphology of the 0.9%Cu/SiO_2–MnO_2 sample was determined by scanning electron microscopy (SEM) and is shown in Fig. S1B, ESI.† The SEM image of the commercial 1%Cu/SiO_2–MnO_2 is also shown in Fig. S1A (ESI†). It was found that its morphology is totally different from that of the hydrothermally prepared 0.9%Cu/SiO_2–MnO_2 catalyst (Fig. S1B, ESI†). The SEM image shows that the particle sizes are almost uniform. The presence of Cu on the SiO_2–MnO_2 support was confirmed by EDAX (energy dispersive analysis by X-ray) analysis and the result is shown in Fig. S1C (ESI†). Elemental mapping of Cu was also performed, and it was found that Cu was homogeneously distributed over the SiO_2–MnO_2 support (Fig. S1D, ESI†). TEM images of the 0.9%Cu/SiO_2–MnO_2 catalyst are shown in Fig. 1B. The average particle sizes of the supported catalyst were found to be between 25 and 50 nm. No Cu particles were imaged by HRTEM, indicating the presence of very small Cu clusters. However, lattice fringes with a *d*-spacing of 3.1 Å corresponding to the (110) lattice plane of hexagonal α-MnO_2 are shown in Fig. 1Bb and Fig. S2, (ESI†). The BET surface area as measured by N_2 adsorption for the 0.9%Cu/SiO_2–MnO_2 was 78 $m^2\ g^{-1}$.

Fig. S3B (ESI†) shows the $Cu_{2p_{3/2}}$ binding energy (BE) peaks. The deconvolution of the peak shows the presence of two different types of Cu species. The BE peak at 934.3 eV shows the presence of Cu^{2+} species and the peak at 932.4 eV shows the presence of either Cu^{1+} or Cu^0, as there is no difference in the Cu^{1+} and Cu^0.[11] However, from EXAFS (extended X-ray absorption fine structure) analysis (discussed later) we could not detect the presence of metallic Cu, so the catalyst contains Cu^{1+} rather than Cu^0. We also noticed that the atomic ratio of Cu^{1+} to Cu^{2+} present in the surface is 9 : 1. Therefore, the surface contains mostly very small nanoclusters of Cu_2O. Furthermore, the $2p_{3/2}$ binding energy value of Mn was observed to be 642.2 eV, along with a separation of 11.4 eV between $2p_{3/2}$ and $2p_{1/2}$, which indicates the presence of Mn^{4+} within the catalyst.[12,13] Fig. S4 (ESI†) shows the TPR profile of 1%Cu/SiO_2–MnO_2^{com} (prepared by an impregnation method) and the 0.9%Cu/SiO_2–MnO_2 catalyst. Three reduction peaks were observed at 236 °C, 338 °C and 426 °C for 0.9%Cu/SiO_2–MnO_2. However, the reduction profile of 1%Cu/SiO_2–MnO_2^{com} also shows three characteristic reduction peaks at 406 °C, 376 °C and 443 °C. We believe that these three peaks are due to the following: (i) reduction of the Cu species (green line), (ii) reduction of Mn^{4+} to Mn^{3+} (red line), and (iii) reduction of Mn^{3+} to Mn^{2+} (blue line), as suggested by the literature.[14] It was also observed that the peaks shifted to lower values for the 0.9%Cu/SiO_2–MnO_2 catalyst compared to 1%Cu/SiO_2–MnO_2^{com}. It has to be noted that, due to the presence of nanocrystalline MnO_2 particles in 0.9%Cu/SiO_2–MnO_2, the peaks for Mn^{4+} and Mn^{2+} appeared at lower values (338 °C and 426 °C) compared to the values for commercial MnO_2 (376 °C and 443 °C). The peak due to Cu appears for 406 °C in the 1%Cu/SiO_2–MnO_2^{com} catalyst, whereas the value shifted to 236 °C for 0.9%Cu/SiO_2–MnO_2. We attributed this peak to the reduction of very small copper oxide nanoclusters.[15] It is easier to reduce small copper oxides rather than the larger particles present in the bulk, due to the diffusion limitation.[16] Therefore, the size of the copper oxide particles is smaller in 0.9%Cu/SiO_2–MnO_2 compared to the bulk 1%Cu/SiO_2–MnO_2^{com}. Commercial MnO_2 does not show any acidity, but SiO_2 shows weak acid sites (Fig. S5A–C; ESI†); however, the as-prepared Cu/SiO_2–MnO_2 catalyst shows a moderate acidity of 149 μmol g^{-1}. We believe that the enhancement of surface acidity is mainly due to the presence of nanocrystalline SiO_2, along with hexagonal MnO_2 (as confirmed by TEM analysis, shown in Fig. S2, ESI†). Earlier reports also revealed that hexagonal MnO_2 is responsible for the generation of acid sites.[17] Therefore, the total acidity arises due to the presence of SiO_2 and hexagonal MnO_2 in the catalyst. The NH_3-TPD pattern of the Cu/SiO_2–MnO_2 (Fig. S4, ESI†) shows a broad peak spanning the temperatures 200–320 °C. Deconvolution of the peak shows the presence of two peaks. We assume that the first peak is due to the presence of SiO_2 and the second peak is due to the presence of hexagonal MnO_2 in the catalyst. It is very clear from the TPD spectra that the second peak is bigger than the first peak, which clearly indicates that the enhancement of the acidic sites is mainly due to the formation of hexagonal MnO_2. The Cu-XANES (X-ray absorption near edge structure) spectra of the fresh and spent Cu/SiO_2–MnO_2 catalysts are shown in Fig. S6 (ESI†); for comparison, the XANES spectra of Cu foil, commercial Cu_2O and CuO are also presented. It is well known that Cu^{1+} compounds exhibit two peaks due to the transition of $1s \rightarrow 4p_{x,y}$ at 8984 eV and $1s \rightarrow 4p_z$ at 8995 eV.[18] Metallic Cu and Cu^{1+} have no hole in the 3d orbital, but Cu^{2+} compounds are in a d^9 configuration, showing a weak pre-edge peak that represents the quadrupole allowed $1s \rightarrow 3d$ transition appearing below the edge. The XANES spectra of the 0.9%Cu/SiO_2–MnO_2 catalyst are not typical of Cu_2O, but are more likely to represent a mixture of Cu_2O and CuO.

Detailed structural parameters of the Cu species were obtained by Cu *K*-edge EXAFS analysis. K^3-weighted Fourier

Transformation of Cu *K*-edge EXAFS spectra are shown in Fig. S7 (ESI†). The curve fitting results are summarized in Table S1 (ESI†). The spectra cannot be fitted as either pure CuO crystals or Cu_2O crystals; they are small crystals of Cu_2O with dispersed CuO. The EXAFS spectra of the fresh (Fig. S7A, ESI†) and spent (Fig. S7B, ESI†) 0.9%Cu/SiO_2–MnO_2 catalyst show the presence of small crystals of Cu_2O with dispersed CuO. For the fresh catalyst, the Cu–O bond length of 1.954 ± 0.152 Å with CN 1.9 ± 0.7 indicates the presence of Cu^{2+} species. The copper oxide nanoclusters over SiO_2–MnO_2 were durable under a glycerol oxydehydration reaction. The structure parameters determined by Cu *K*-edge EXAFS for 0.9%Cu/SiO_2–MnO_2 after the glycerol oxydehydration indicate that there is no significant change in the structure of the nanoclusters after 30 h reaction time (spent catalyst, Table S1, ESI†). The Cu–O bond length of 1.951 ± 0.113 Å with CN of 1.7 ± 0.6 shows that the size of the nanoclusters is almost the same, even after the reaction. Furthermore, EXAFS analysis confirms that there were no Cu–Cu bonds present in the catalyst. This clearly indicates that Cu^0 (metallic copper) is not present in our catalyst.

The activities of the different Cu-catalysts are shown in Table 1. Oxydehydration of glycerol over the 0.9%Cu/SiO_2–MnO_2 catalyst shows acrylic acid and acrolein as the main products, along with the formation of a small amount of 3-hydroxypropionaldehyde. A glycerol conversion of 77.1% with 74.7% acrylic acid selectivity (entry 4) was achieved over the 0.9%Cu/SiO_2–MnO_2 catalyst after 30 h reaction time, with a TOF (turnover frequency) value of 32.9 h^{-1}. Commercial MnO_2 (entry 1) gives only 5.5% glycerol conversion, without any formation of acrylic acid. 1%Cu supported on SiO_2–MnO_2 (prepared by physical mixing) also shows negligible selectivity for acrylic acid (entry 3). MnO_2 prepared by a hydrothermal method also shows low activity (8.6% conversion and 5.6% acrylic acid selectivity, entry 2). Catalysts of Cu supported on MnO_2 or SiO_2 (entries 7 & 8) also do not show any activity.

Table 1 Activity of the Cu/SiO_2–MnO_2 catalyst[a]

Sl. no.	Catalyst	χ_G[d] (%)	Selectivity (C %) AA	3HPA	AC	OT	TOF (h^{-1})	E_o
1	MnO_2[com]	5.5	0.1	2.8	3.1	~94.0	—	~0
2	MnO_2	8.6	5.6	2.5	1.8	~90.1	—	0.09
3	1%Cu/SiO_2–MnO_2[com]	9.7	3.4	3.0	3.5	90.1	—	0.06
4	0.9%Cu/SiO_2–MnO_2	77.1	74.7	6.8	10.4	8.1	32.9	11.52
5	0.9%Cu/SiO_2–MnO_2[b]	72.5	72.0	5.8	11.6	10.6	30.7	10.52
6	0.9%Cu/SiO_2–MnO_2[c]	100	100	—	—	—	—	20.0
7	1%Cu/MnO_2	8.3	0	4.1	4.8	91.1	—	—
8	1%Cu/SiO_2	7.7	0	3.7	12.9	83.4	—	—

[a] Catalyst: 0.046 g; glycerol: 0.92 g in 10 mL CH_3CN, temperature: 70 °C; substrate (glycerol): 50% H_2O_2 (1 : 5, molar ratio). [com] commercial oxide. [b] After 4 successive runs under the same conditions. [c] With acrolein as the substrate after 3 h reaction time. [d] In mol%. TOF: moles of acrylic acid produced per moles of Cu per unit time; E_o: H_2O_2 efficiency calculated by (100 × moles of acrylic acid formed)/total moles of H_2O_2 added; C balance was carried out for most of the experiments and the value was within 98–102%. χ_G = conversion of glycerol (C%), AA = acrylic acid, AC = acrolein and OT = others.

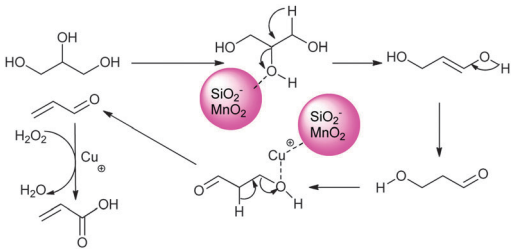

Scheme 1 Probable mechanistic pathway for the conversion of glycerol to acrylic acid.

Therefore, the presence of Cu nanoclusters and the presence of acid sites (due to SiO_2 and MnO_2) are the two key factors for the oxydehydration of glycerol. A probable mechanistic pathway for the formation of acrylic acid is shown in Scheme 1. The catalyst behaves as a bifunctional catalyst, where the SiO_2 and the hexagonal MnO_2 sites act as acidic sites responsible for the dehydration reaction (glycerol to acrolein), and the Cu^+ sites are responsible for the oxidation reaction (acrolein to acrylic acid). Based on the results obtained, we believed that the reaction goes through at least two intermediates: 3-hydroxypropionaldehyde and acrolein. Here, the first step is the dehydration of glycerol to form 3-hydroxypropionaldehyde over the acid sites of the catalyst. The second step is also a dehydration reaction, this time of the 3-hydroxypropionaldehyde to form acrolein. Finally the acrolein oxidizes to form acrylic acid in the presence of H_2O_2 (50% in H_2O) over the Cu sites. To check the intermediate acrolein formation, we performed the experiment using acrolein as the substrate, and found that both acrolein conversion and acrylic acid selectivity was 100% within 3 h (entry 6). We believe that the dehydration step is very slow, but the oxidation step is very fast. Initially it takes a long time to form acrylic acid. However, once acrylic acid formation begins, it acts as a Brønsted acid in the reaction mixture, and the rate of acrylic acid formation increases. The increase in the H_2O_2 : glycerol (Fig. S8, ESI†) molar ratio does not have any substantial effect on acrylic acid selectivity, as it remains almost the same. A noticeable increase in glycerol conversion from 49.9% to 77.1% was observed when the glycerol to H_2O_2 molar ratio increased from 2.5 to 5; whereas the conversion decreased from 77.1% to 70.1% with a further increase in the glycerol to H_2O_2 molar ratio, to 7.5. It seems that with an increase in the H_2O_2 molar ratio the decomposition of H_2O_2 increases, so the glycerol conversion decreases. The effect of temperature is shown in Fig. 2A. It was found that the glycerol conversion increases continuously with temperature but that the selectivity decreases above 70 °C. We believe that above 70 °C, the decomposition of H_2O_2 takes place, and so the selectivity decreases. The effect of reaction time is shown in Fig. 2B. It was observed that both the glycerol conversion and acrylic acid selectivity continuously increased when the reaction time was increased from 10 to 30 h, but that the selectivity decreased after 30 h.

The reusability of the 0.9%Cu/SiO_2–MnO_2 catalyst was studied without any regeneration. The catalyst showed almost the same activity even after four successive runs under the same

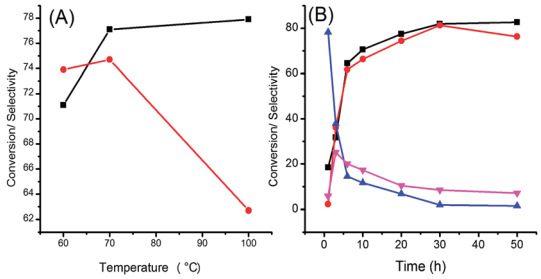

Fig. 2 (A) Effect of reaction temperature and (B) effect of reaction time (h) as a function of glycerol oxidation when 0.046 g catalyst and 0.92 g glycerol in 10 ml solvent were stirred at 70 °C. [■] Glycerol conversion; [●] selectivity to acrylic acid; [▼] selectivity to acrolein and [▲] selectivity to 3HPA.

reaction conditions. The catalyst showed 72.8% conversion and 72.1% acrylic acid selectivity after 4 cycles (entry 5, Table 1). The small decrease in activity could be mainly due to the unavoidable loss of catalyst during washing. The ICP-AES analysis of the fresh and spent catalyst after four successive cycles confirms that there was no leaching of Cu metal from the catalyst. This also supports the heterogeneity of the catalyst.

In summary, we have found Cu nanoclusters supported on SiO_2–MnO_2 to be a very efficient catalyst for the direct conversion of glycerol to acrylic acid using hydrogen peroxide as an oxidant. A glycerol conversion of 77.1% with 74.7% acrylic acid selectivity was achieved after 30 h reaction time. The Cu species could not be detected by XRD or TEM, but an EXAFS study revealed the formation of Cu nanoclusters on the MnO_2 support. Cu nanoclusters and nanocrystalline SiO_2–MnO_2 are the key parameters for high conversion and selectivity in the oxydehydration of glycerol. The reusability of the catalyst was tested by conducting 4 successive runs with the same catalyst. The catalyst showed similar glycerol conversion with the same acrylic acid selectivity, confirming the reusability of the catalyst.

B.S. acknowledges the University Grant Commission (UGC), India for the fellowship. R. B. thanks CSIR, New Delhi for the financial support in the form of the 12 FFYP (CSC-0117 and CSC-0125). We also acknowledge the Director of CSIR-IIP for his support. The authors thank the Analytical Science Division, Indian Institute of Petroleum for analytical services. The XAFS measurements were performed at KEK-IMSS-PF with the approval of the Photon Factory Advisory Committee (project 2010G109).

Notes and references

1 (*a*) W. S. Broecker, T. Takahashi, H. J. Simpson and T. H. Peng, *Science*, 1979, **206**, 409; (*b*) P. D. Quay, B. Tilbrook and C. S. Wong, *Science*, 1992, **256**, 74; (*c*) S. Dahl and I. Chorkendorff, *Nat. Mater.*, 2012, **11**, 100.

2 (*a*) C. H. Zhou, J. N. Beltramini, Y. X. Fan and G. Q. Lu, *Chem. Soc. Rev.*, 2008, **37**, 527; (*b*) F. Jerome, Y. Pouilloux and J. Barrau, *ChemSusChem*, 2008, **1**, 586; (*c*) A. Corma, S. Iborra and A. Velty, *Chem. Rev.*, 2007, **107**, 2411; (*d*) G. W. Huber, R. D. Cortright and J. A. Dumesic, *Angew. Chem., Int. Ed.*, 2004, **43**, 1549; (*e*) G. W. Huber, J. W. Shabaker and J. A. Dumesic, *Science*, 2003, **300**, 2075; (*f*) C. Pendem, P. Gupta, N. Chaudhary, S. Singh, J. Kumar, T. Sasaki, A. Datta and R. Bal, *Green Chem.*, 2012, **14**, 3107.

3 Glycerol, , *Glycerol, Kirk-Othmer Encyclopedia of Chemical Technology*, John Wiley & Sons, Inc., New York, 2001.

4 (*a*) S. H. Lee, S. J. Park, O. J. Park, J. Cho and J. W. Rhee, *J. Microbiol. Biotechnol.*, 2009, **19**, 474; (*b*) S. Kudla and M. Kaledkowska, *Przem. Chem.*, 1998, **77**, 86; (*c*) P. A. Glubish, *Use of Polymers of Acrylic Acid and Its Derivatives in the Textile and Light Industries*, 1975, p. 205; (*d*) P. C. Chromecek, W. G. Deichert, J. J. Falcetta and M. F. VanBurn, *US pat.*, 4276402, 1981.

5 (*a*) Y. T. Kim, K. D. Jung and E. D. Park, *Appl. Catal., B*, 2011, **107**, 177; (*b*) E. Tsukuda, S. Sato, R. Takahashi and T. Sodesawa, *Catal. Commun.*, 2007, **8**, 1349.

6 (*a*) S. H. Chai, H. P. Wang, Y. Liang and B. Q. Xu, *J. Catal.*, 2007, **250**, 342; (*b*) A. Ulgen and W. Hoelderich, *Catal. Lett.*, 2009, **131**, 122; (*c*) W. Suprum, M. Lutecki, T. Haber and H. Papp, *J. Mol. Catal. A: Chem.*, 2009, **309**, 71; (*d*) Y. T. Kim, K. D. Jung and E. D. Park, *Microporous Mesoporous Mater.*, 2010, **131**, 28; (*e*) A. Corma, G. W. Huber, L. Sauvanaud and P. O'Connor, *J. Catal.*, 2008, **257**, 163.

7 (*a*) M. Shima, K. Shi and T. Takahashi, *EU pat.*, EP1710277B1, 2005; (*b*) J. L. Dubois, *Pat. App. No.*, 20100168471 (AC07C5116FI), 2010; (*c*) J. L. Dubois, C. Duquenne and W. Holderich, *US Pat.*, 7910771, 2011; (*d*) S. H. Chai, H. P. Wang, Y. Liang and B. Q. Xu, *Green Chem.*, 2008, **10**, 1087.

8 (*a*) M. D. Soriano, P. Concepcion, J. M. L. Nieto, F. Cavani, S. Guidetti and C. Trevisanut, *Green Chem.*, 2011, **13**, 2954; (*b*) F. Wanga, J. L. Duboisb and W. Ueda, *J. Catal.*, 2009, **268**, 260.

9 (*a*) B. Sarkar, P. Prajapati, R. Tiwari, R. Tiwari, S. Ghosh, S. S. Acharyya, C. Pendem, R. K. Singha, L. N. S. Konathala, J. Kumar, T. Sasaki and R. Bal, *Green Chem.*, 2012, **14**, 2600; (*b*) S. S. Acharyya, S. Ghosh, R. Tiwari, B. Sarkar, R. K. Singha, T. Sasaki, C. Pendem and R. Bal, *Green Chem.*, 2014, **16**, 2500.

10 Z. Y. Yuan, Z. Zhang, G. Du, T. Z. Ren and B. L. Su, *Chem. Phys. Lett.*, 2003, **378**, 349.

11 C. D. Wagner, A. V. Naumkin, A. K. Vass, J. W. Allison, C. J. Powell and J. R. Rumble, Jr., *NIST Standard Reference Database 20*, Version 3.4, (web version) (http://srdata.nist.gov/xps/), 2003.

12 (*a*) A. A. Mirzaei, H. R. Shaterian and M. Kaykhaii, *Appl. Surf. Sci.*, 2005, **239**, 246; (*b*) H. Y. Chen, J. Lin, K. L. Tan and J. Li, *Appl. Surf. Sci.*, 1998, **126**, 323; (*c*) F. Marquez, A. E. Palomares, F. Rey and A. Corma, *J. Mater. Chem.*, 2001, **11**, 1675; (*d*) M. Diab, B. Moshofsky, I. J. La-Plante and T. Mokari, *J. Mater. Chem.*, 2011, **21**, 11626.

13 C. D. Wagner, W. M. Riggs, L. E. Davis, J. F. Moulder and G. E. Muilenberg, *Handbook of X-ray Photoelectron Spectroscopy*, Perkin-Elmer Corp., Eden Prairie, USA, 1979.

14 S. Liang, F. Teng, G. Bulgan, R. Zong and Y. Zhu, *J. Phys. Chem. C*, 2008, **112**, 5307.

15 Z. Ma, Z. Xiao, J. A. van Bokhoven and C. Liang, *J. Mater. Chem.*, 2010, **20**, 755.

16 R. Rajeev, K. A. Devi, A. Abraham, K. Krishnan, T. E. Krishnan, K. N. Ninan and C. G. R. Nair, *Thermochim. Acta*, 1995, **254**, 235.

17 Z. R. Tian, W. Tong, J. Y. Wang, N. G. Duan, V. V. Krishnan and S. L. Suib, *Science*, 1997, **276**, 926.

18 (*a*) J. Y. Kim, J. A. Rodriguez, J. C. Hanson, A. I. Frenkel and P. L. Lee, *J. Am. Chem. Soc.*, 2003, **125**, 10684; (*b*) W. B. Kim and J. S. Lee, *J. Phys. Chem. B*, 2003, **107**, 9195.

